Regolith excavation performance of a screw-propelled vehicle

Marko Green[1], Teresa McBryan[1], Darwin Mick[1], David Nelson[1], Hamid Marvi[1*]

1 School for Engineering of Matter, Transport and Energy, Arizona State University, Tempe, AZ, USA

* hmarvi@asu.edu

Abstract

Excavation of regolith is the enabling process for many of the in-situ resource utilization (ISRU) efforts that are being considered to aid in the human exploration of the moon and Mars. Most proposed planetary excavation systems are integrated with a wheeled vehicle, but none yet have used a screw-propelled vehicle which can significantly enhance the excavation performance. Therefore, CASPER, a novel screw-propelled excavation rover is developed and analyzed to determine its effectiveness as a planetary excavator. The excavation rate, power, velocity, cost of transport, and a new parameter, excavation transport rate, are analyzed for various configurations of the vehicle through mobility and excavation tests performed in silica sand. The optimal configuration yielded a 30 kg/hr excavation rate and 10.2 m/min traverse rate with an overall system mass of 3.4 kg and power draw of less than 30 W. These results indicate that this architecture shows promise as a planetary excavation because it provides significant excavation capability with low mass and power requirements.

Introduction

In-situ space excavation is a highly researched and sought after branch of technology as it will enable numerous scientific and exploration goals. In the lunar case, the ability to excavate will enable in-situ construction of a lunar base using novel additive manufacturing techniques.[1–3] Furthermore, continued examination of lunar regolith and its geological history can give key information to the rotation history of the Sun.[4] Additionally, lunar ice in permanently shaded regions of the moon can be harvested for use in propulsion systems.[5–8] Overall, In-situ Resource Utilization (ISRU), especially on the moon, will make space more accessible and can enable a sustained human presence.[9–14]

As explained by Just et al.,[15] there are several ways to classify excavators. First, it must be determined if the excavation method is discrete or continuous. A discrete method breaks contact with regolith in order to dump or store the collected material, effectively taking one large sample at a time. On the other hand, a continuous excavation system uses many cutting surfaces that successively make contact with the regolith.[16] So, as one surface moves to store the collected sample, another surface has started collecting allowing the excavator to maintain contact with the regolith continuously. Furthermore, systems can be classified as either partial or complete. A partial system is just an excavation system, whereas a complete system has the excavation mechanism included as a part of an overall mobility platform. They also conclude that three main parameters should be measured when comparing these systems:

- **Excavation rate:** The frequency at which regolith is collected.
- **Traverse rate:** The maximum speed of the mobility system.
- **Power consumption:** The amount of power consumed by the entire system, not just the excavation.
- **Properties of simulant/analogue used:** The properties of the material used as an analogue for the real-world use case.

These parameters are indeed critical to characterizing the performance of ISRU excavation systems, however, this paper will examine two additional parameters that provide further insight into system performance: the cost of transport (COT), which is a measure of mobility efficiency and the excavation transport rate (ETR), a new parameter introduced in this work that seeks to combine excavation and mobility performance. In particular, ETR is the rate at which the excavation system collects material, normalized by the craft mass and cost of transport.

All research to this effect has focused primarily on wheeled excavation systems and other mobility modes such as screw-driven mobility that can directly benefit excavation have not been much explored. For example, Scarab is a prototype lunar rover that utilizes a drill to excavate material. However, the mobility platform for this craft is wheeled and uses the same rocker-bogie suspension system found on Mars rovers.[17,18] Moreover, prototype rovers such as MAMMOTH and Sherpa both seek to innovate with their novel active suspensions, but conduct these studies using only one wheel type.[19,20] Work has also been conducted to better understand grousered wheel interactions with regolith.[21] Furthermore, studies into the excavation force requirements for space environments are conducted.[22] This insight, coupled with the low weight and traction forces experienced in space imply that the excavation system should minimize the excavation force, and maximize the amount of traction provided by the mobility system in order to enable efficient excavation for ISRU.[23] Nonetheless, the effect of wheel design and mobility system on excavation has not been studied.

Screwed-Propelled Vehicles (SPVs) use pontoons with helical protuberances that dig through granular media. This displaces the media and pushes the vehicle forward. They have traditionally been used in terrestrial applications in amphibious or otherwise challenging environments[24–26] where marshes, clay, or ice are present. These environments prevent vehicles using wheels or tracks from being reliably mobile. However, SPVs are well suited to those terrains because they are mechanically simple, provide a large surface area for traction, and work in both dry and wet conditions. Screw generated forces in granular media have been analyzed both experimentally and computationally.[27, 28] Furthermore, screw-driven mobility platforms have been tested in a lunar regolith analogue and computationally tested using gravity variant coupled discrete element method and multi-body dynamics simulations.[29–32] Results indicate that screw propelled vehicles work well across a wide range of gravities. In addition, scaling laws have been developed that relate gravity and craft size to the craft's velocity and power draw.[29–32] Building upon this prior body of work, a screw-propelled excavation rover is developed and serves as the test subject for this analysis. This vehicle aims to meet the requirements of in-space excavation by using the screw propulsion system to provide high tractive force and reduce excavation force through churning the granular media and reducing its compaction.

The Counter-rotating Archimedes Screw-Propelled Excavation Rover (CASPER) is a novel platform that combines screw-propelled mobility with a discrete scooper excavation method. CASPER uses four screws to move itself forward while a centrally located ramp excavates material during rover movement. This combination of excavation technique augmented by a screw mobility system has not been investigated before, and will be compared to other techniques using the parameters described above. We will first discuss the design of the CASPER rover and the experimental procedures. Next we will present our experimental data on CASPER mobility and excavation performance. Finally, we will conclude with the major takeaways from this analysis and potential future directions.

Materials and Methods

Design of CASPER

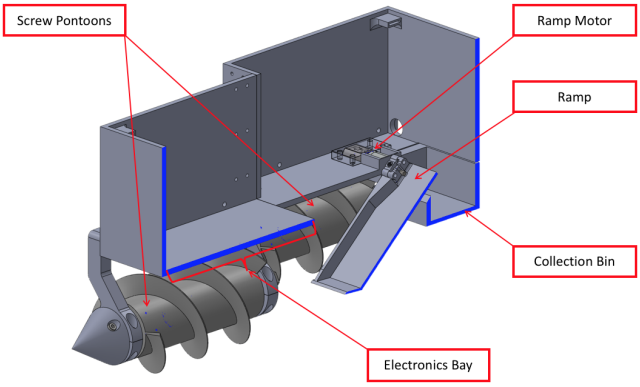

Figure 1. Isometric section view of CASPER with key features labeled.

CASPER is a screw-propelled discrete scooper excavation robot (Figure 1). It is driven by a system of four counter-rotating Archimedes screw pontoons. Each of these pontoons are driven by an internal 12 V DC motor which is sealed against sand ingress. The pontoons serve primarily as the mobility system, but also play a key role in the excavation system. The excavation system consists of two major components, the pontoons, and the ramp. The pontoons churn up the material and propel the ramp forward, while the actuated ramp collects the material and rotates to deposit the material into the collection bin. The majority of CASPER parts were 3D printed in PETG on an FDM 3D printer.

A Raspberry Pi was used to control all craft functions and collect experimental data. The screw pontoons were each powered by a 75:1 DC gear motor (Pololu; item #4846) and the ramp was actuated using a 488:1 DC gear motor (Polulu; item #3723). The ramp required a very high gear ratio motor because it needed to be able to maintain the desired angle while experiencing very high drag forces from the granular media. Each motor comprised of a motor, gearbox, encoder, current sensor, and a motor controller for speed control. The craft was tethered to and powered by an external power supply providing a constant voltage of 12 V to the system. A proportional-derivative (PD) controller was utilized to regulate pontoon speeds to ensure accurate speed control and was tuned such that the craft consistently achieved steady state in approximately 0.9 - 1.3 seconds for all screw angular velocity settings. This guaranteed that the craft would be at steady state when the ramp excavation procedure began at 2 seconds after run start.

Table 1. Experimental Configuration Parameters

Configuration	Front pontoon width	Churn direction	ω (RPM)	Load time	Ramp angle
C1	145 mm (Wide)	Outward	20, 30, 40	0 s, 2 s, 4 s, 6 s	0 °, 35°, 40°, 45°
C2	145 mm (Wide)	Inward	20, 30, 40	0 s, 2 s, 4 s, 6 s	0 °, 35°, 40°, 45°
C3	105 mm (Narrow)	Outward	20, 30, 40	0 s, 2 s, 4 s, 6 s	0 °, 35°, 40°, 45°
C4	105 mm (Narrow)	Inward	20, 30, 40	0 s, 2 s, 4 s, 6 s	0 °, 35°, 40°, 45°

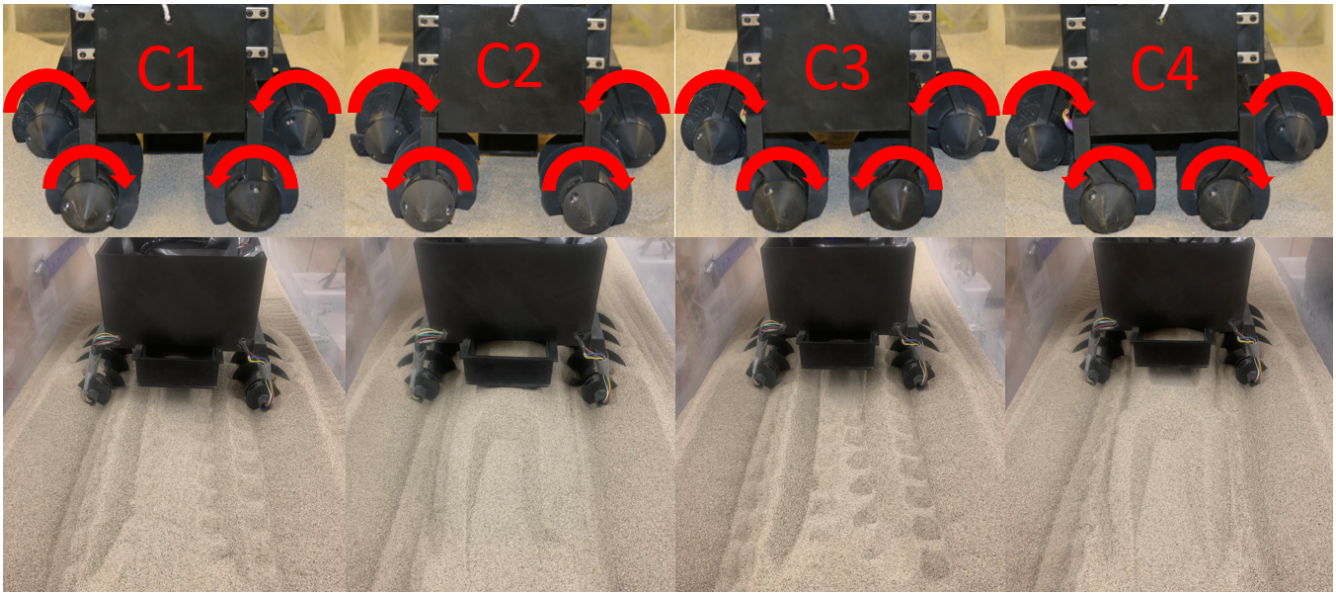

Figure 2. Front view of each configuration with indicated screw rotation direction and their corresponding wakes.

Four major configurations of CASPER were tested during the course of this research. The parameters of each configuration are detailed in Table 1 and the physical layout, rotation directions, and wake images are shown in Figure 2. Each configuration had a unique combination of front pontoon width (narrow or wide), and the direction in which material was churned by the front pontoons (inward or outward). Configurations C1 and C2 (pictured in Figure 2) have pontoon mounts that create a 145 mm separation between the centers of the front pontoons, while the C3 and C4 configurations have a narrow set of pontoon mounts that create 105 mm of separation. Furthermore, the even configurations C2 and C4 have front pontoon handedness and rotation direction opposite of the rear screws, which causes the material to be churned inward by the front pontoons. This "inward churning" creates a wake of loosely compacted material that is elevated with respect to the undisturbed sand, which enables the ramp to easily scoop the material in discrete amounts. Conversely, the odd configurations C1 and C3 have identical screw handedness and rotation direction as the rear pontoons, which causes the material to be churned outward and away from the central ramp. For each configuration, the power, velocity, and excavation rate of the craft were investigated over a range of each of the following independent variables:

- **Angular velocity ω:** The rotation rate of each screw pontoon.
- **Load time:** The length of time where the ramp is in the downward fixed position, embedded in the granular media, moving forward, and collecting material.
- **Ramp angle:** The angle that the ramp surface makes with respect to the floor of the craft body.

It should be noted that the 0° ramp angle and 0 second load time cases act as the control group for the mobility

power and velocity. This is because during these specific runs, the ramp was disabled in the upright stowed position, so the power and velocity were unaffected by reaction forces due to the ramp excavation.

The purpose of these experiments is to determine what effect, if any, the material churn direction and front pontoon width have upon the power consumption, velocity, and excavation rate of the craft across a wide variety of screw angular velocities, load times, and ramp angles.

Experimental Setup and Procedure

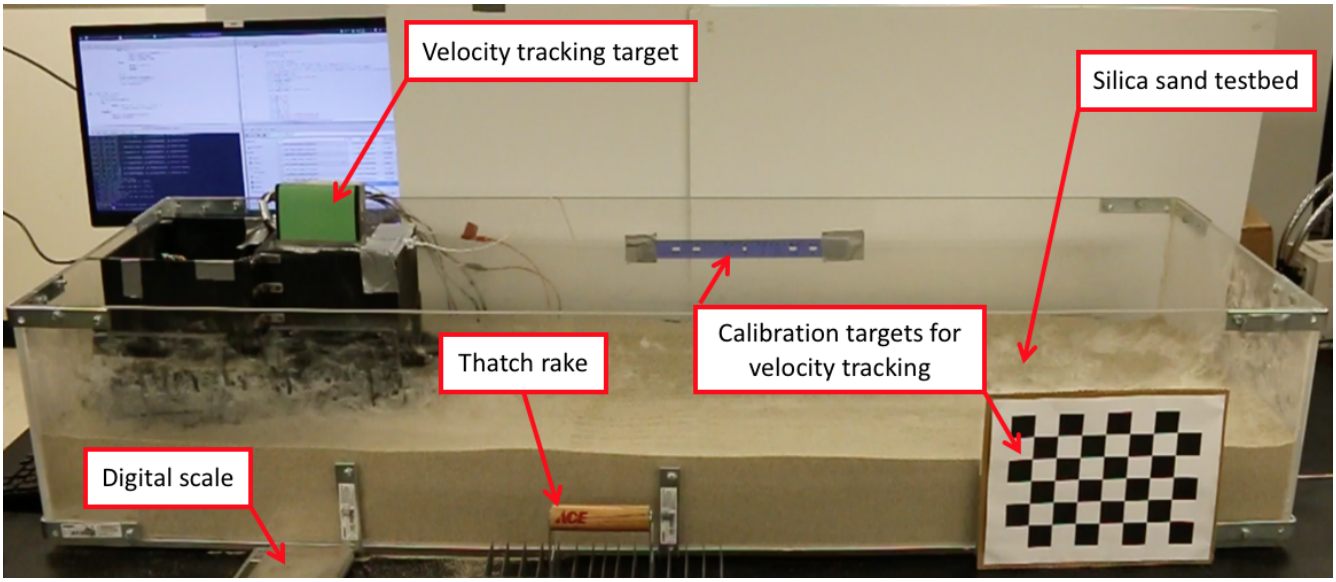

Figure 3. Experimental setup with key equipment labeled.

The experiments were performed in a 150 cm x 45 cm x 45 cm acrylic box (Figure 3) filled with commercially available Quikrete 1962 Eglin silica sand that has a mean particle diameter of 0.8-1.8 mm.[33] Quikrete is a very common granular media to perform mobility experiments in and this is a legacy test bed from past experiments.[29–32] Quikrete silica sand was added to the test bed such that there was 20 cm of depth in order to prevent any wall effects from occurring between the screws and the bottom of the test bed. Prior to each trial, the sand was reset manually using a modified thatch rake using a strictly consistent procedure. This was done to minimize the variance in measured quantities due to a buildup of plastic deformation in the sand. It has been shown that inconsistent soil conditions cause variability in the interactions of the mobility system and the granular media,[34] which increases variance in the measured performance parameters. First, the craft would be removed from the soil. Next, the tines of the thatch rake would be drawn in longitudinal and transverse directions repeatedly until the sand was no longer compacted. Finally, the sand level was checked to make sure that the volume fraction of the sand remained constant between trials.

Once the sand was reset, the craft was replaced at the end of the test bed, and the ramp angle was set using

a digital angle gauge and manual inputs to the craft's control system. After this process, the camera was set to record and the control script was launched at the command line to start the run. The craft was then allowed to traverse forwards until the ramp had deposited two discrete scoops into the collection bin, thus concluding the run. Two scoops were chosen because this is the maximum amount of scoops possible in this length of a test track at the highest screw angular velocity of 40 RPM with the longest load time of 6 seconds. Finally, the collection bin was removed and weighed using a digital scale and the resulting value was recorded. After recording the mass, the process was repeated for a multiplicity of five trials per experimental configuration.

The RPM, voltage, and current data vectors for each of the five motors were analyzed in MATLAB. For each trial, the current and voltages of each motor were multiplied together to obtain the electrical power supplied to the DC motors. Next, the time average of the power curves were taken across the temporal range where the craft had reached steady state, as indicated by the RPM versus time curve. The time-average power values for all five trials were recorded, and the ensemble average of these values was taken to determine the average power consumption for that specific set of experimental parameters.

Next, the videos of each run were analyzed using a color tracking MATLAB script. The camera was calibrated by taking several images of the checkerboard, including ones planar to the green color tracking target, and analyzing them in MATLAB to get the camera's intrinsic and extrinsic parameters. This enabled the pixel coordinates to be converted into world coordinates. The script analyzed each video frame by frame, finding the location of the center of the green target and thus, giving distance over time and therefore velocity. The average velocity was then calculated by taking the time-average of the velocity over the duration where the craft was considered in steady state. The values for all five trials were taken and averaged together to get an average velocity for that specific set of experimental parameters.

Results and Discussion

As mentioned in the previous section, the purpose of these experiments was to quantify the effect the material churn direction and front pontoon width have upon the power consumption, velocity, and excavation mass performance of the craft across a wide variety of screw angular velocities, load times, and ramp angles. In the following subsections, the experimental data for the excavation rate, power, velocity, cost of transport, and excavation transport rate are presented and analyzed.

Excavation Rate

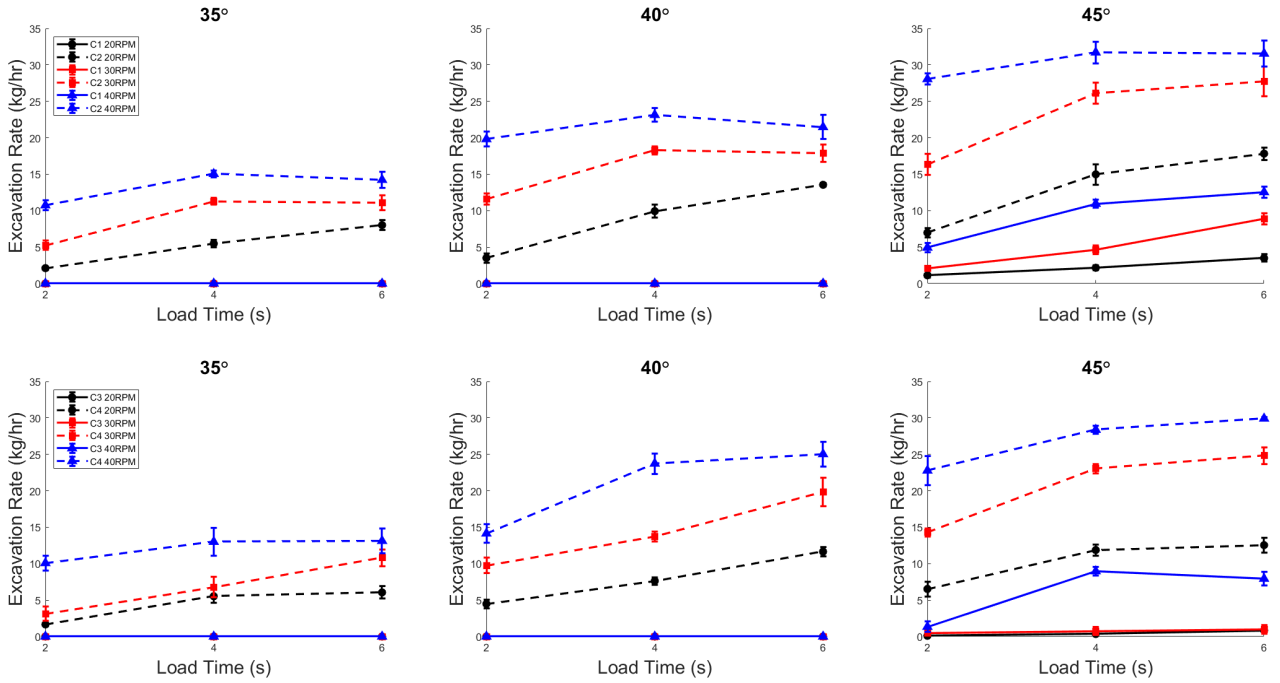

Figure 4. Comparison of average excavation rate (kg/hr) vs. load time (s) between all configurations for ramp angles of 35°, 40°, and 45°, and screw rotational velocities of 20, 30, and 40 RPM.

Upon examining results presented in Figure 4, it is evident that the excavation rate behavior of CASPER is relatively well behaved insofar as it exhibits similar quasi-linear trends across all independent variables. For both the wide and narrow outward churning configurations C1 and C3, the ramp system was unable to collect any granular media at ramp angles of 35° and 40°. Even at 45°, C1 and C3 were only able to excavate at 40 RPM, the fastest angular velocity tested. This illustrates the superiority of the inward churning configurations with respect to the excavation capability. In addition, the ramp motor requires less angular displacement and thus, less work to deposit the material in the collection bin.

Unsurprisingly, the excavation rate increases as the screw angular velocity increases. This is because there is a greater mass flux of granular media flowing onto the ramp edge, which allows the material to build up to a greater height on the blade itself prior to the ramp rotation. For similar reasons, the excavation rate increases as the load time increases. By increasing the load time, the granular media is given more time to build up prior to ramp rotation. It appears that there is a bit of a diminishing returns phenomenon with respect to load time. In other words, the increase from two to four seconds in load time yields a much higher marginal increase in excavation rate in comparison to the marginal increase from four to six seconds.

Power

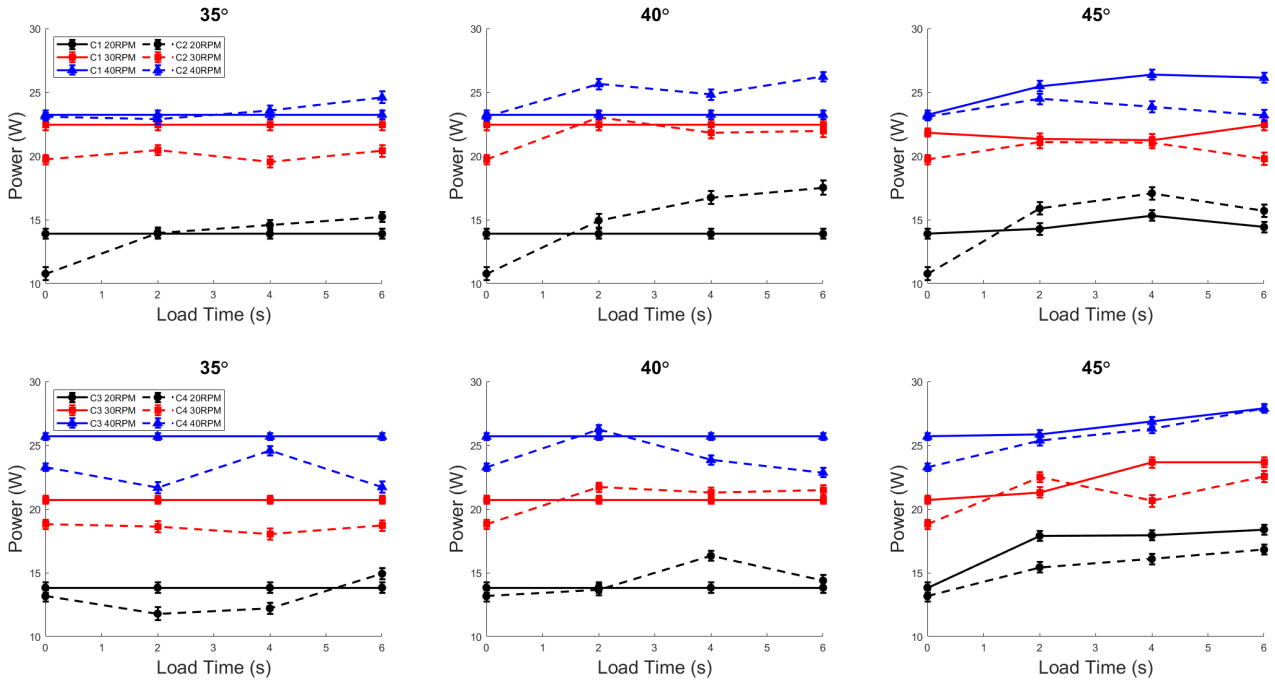

Figure 5. Comparison of average total power (w) vs. load time (s) between all configurations for ramp angles of 0°, 35°, 40°, and 45°, and screw rotational velocities of 20, 30, and 40 RPM.

Figure 5 illustrates that the total power does increase significantly as the screw angular velocities are increased. The 20 RPM total power draw is approximately 15-18 W, while the 40 RPM power draw is roughly 25-28 W, so the increase in power is quasi-linear with respect to RPM. Less intuitively, the power was found to be approximately constant with minor fluctuations with respect to the load time for a given configuration and angular velocity. Initially it was hypothesized that the drag force generated by the ramp-terrain interaction would lead to higher power draw to maintain the velocity, but this was found to not be the case. In all cases where the ramp does not make contact with the soil (C1 and C3 at 35° and 40°), the power draw is nearly identical to the no ramp control case (0 seconds load time). When the ramp does make contact with the soil, the power draw increases slightly above the no ramp level.

It should be noted that the four motors powering the screws consumed the overwhelming majority of the power in all cases. The DC motor actuating the ramp had an astoundingly low power draw of between 0.1-0.2 W, which is one percent of total power. This insight, coupled with the fact that higher load times do not impose a significant power increase, imply that the most efficient configuration in terms of power per unit excavation rate for this system is the one that maximizes the excavation rate. In order to further investigate this hypothesis, the excavation transport rate (ETR) was analyzed, and the results are discussed in a later section.

Velocity

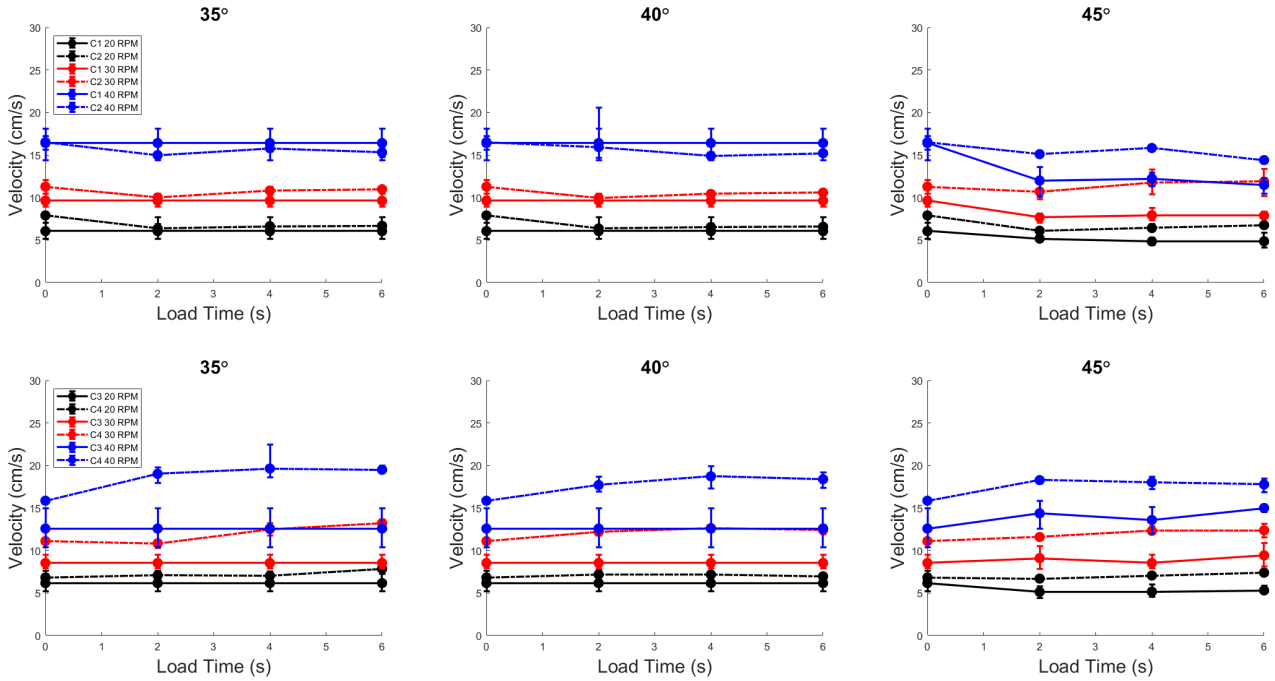

Figure 6. Comparison of average craft velocity vs. load time (s) between all configurations for ramp angles of 35°, 40°, and 45°, and screw rotational velocities of 20, 30, and 40 RPM.

The craft velocity is a very relevant quantity when considering the performance of an excavation vehicle because it is highly correlated to the excavation rate. The velocity distribution of CASPER is presented in Figure 6. Predictably, as the angular velocity of the screws increases, the linear velocity of the craft increases. This pattern has been demonstrated in the literature[28–31] and serves as a sanity check for the velocity results. It is readily apparent that the velocity is fairly constant with respect to load time, as well as ramp angle.

There does not seem to be a significant difference between the wide configurations C1 and C2. However, an interesting disparity exists between the narrow configurations C3 and C4 where the inward churning configuration C3 attains significantly higher velocities than the outward churning C4. This could potentially be explained by how the front pontoon width changes the position of the front pontoon wake. In the wide configurations, the front pontoons are only slightly narrower than the rear pontoons. As a result, the rear pontoons are constantly engaging in media that has already been churned. Conversely, in the narrow configurations, the front pontoons are almost entirely out of the way of the rear pontoons. When churning inward, the rear pontoons are engaging with essentially undisturbed granular media, and thus produce more thrust force than the outward churning case. This effect is likely also present in the wide configuration, but has less impact regardless of the churn direction due to the fact that the front and rear pontoons are nearly in line with each other.

Cost of Transport

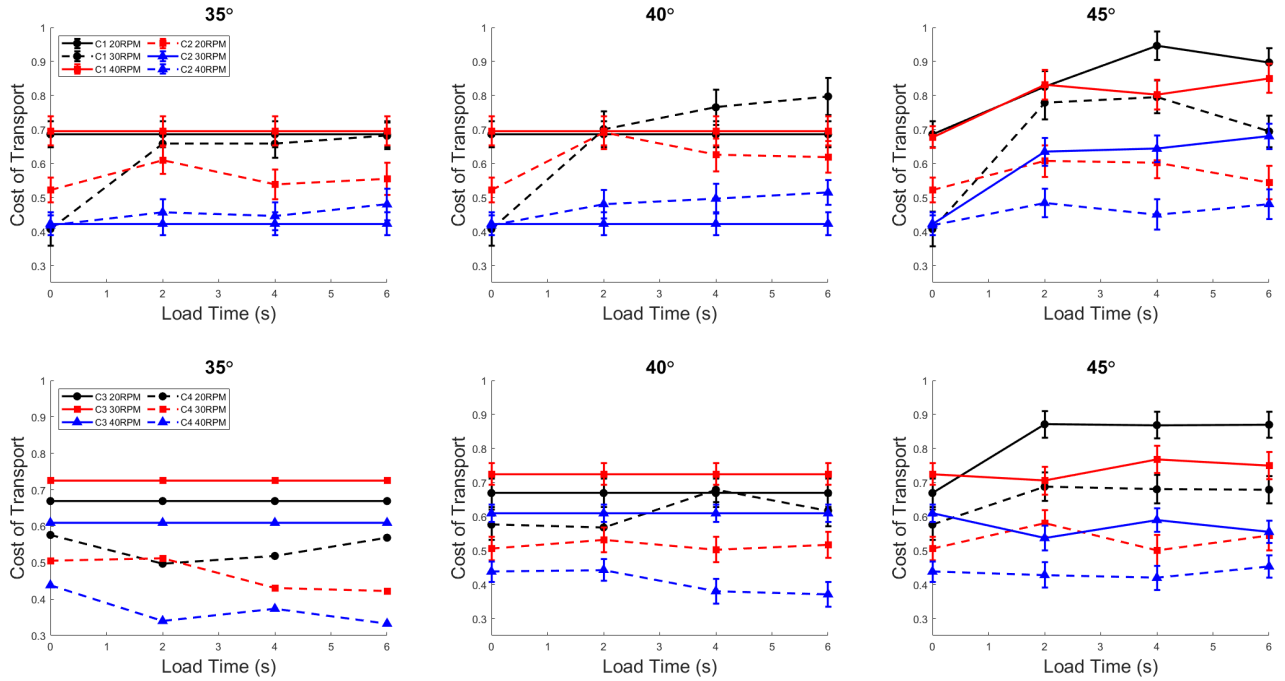

Figure 7. Comparison of average cost of transport vs. load time (s) between all configurations for ramp angles of 35°, 40°, and 45°, and screw rotational velocities of 20, 30, and 40 RPM.

The cost of transport (COT) was analyzed in order to quantify the mobility performance of CASPER. The cost of transport is defined in Equation 1, where P, W_c, and V are the craft power, weight, and velocity, respectively.

$$COT = \frac{P}{W_c \cdot V} \tag{1}$$

Figure 7 shows how the cost of transport varies across all independent variables. Generally, the cost of transport reduces as the RPM increases. Note that the cost of transport is not significantly impacted by load time. Comparing the top and bottom rows of Figure 7, it is clear that the narrow/wide configurations have roughly the same cost of transport at all angular velocities and load times. From these graphs, it can be concluded that higher angular velocities of 30 and 40 RPM yield the lowest cost of transport. This implies that they move the fastest for a given amount of power, and thus are more efficient for mobility in granular media. In the next section, the cost of transport and excavation rate will be investigated simultaneously to quantify the mobility and excavation performance as a whole.

Excavation Transport Rate

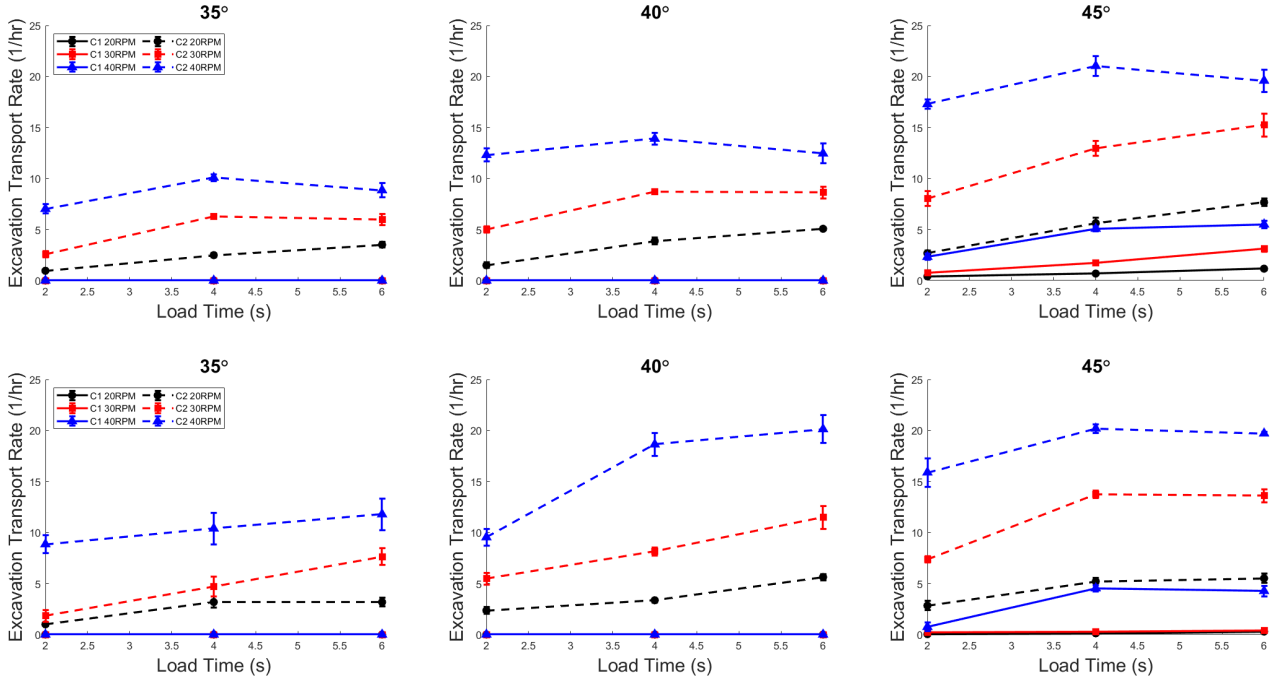

Figure 8. Comparison of average excavation rate/cost of transport vs. load time (s) between all configurations for ramp angles of 35°, 40°, and 45°, and screw rotational velocities of 20, 30, and 40 RPM

The excavation transport rate (ETR) is a new parameter we introduce that can represent the overall transportation and excavation efficiency of a hybrid mobility-excavation system. ETR is defined in Equation 2, where R_E is the excavation rate, m_c is the craft mass, and COT is the cost of transport.

$$ETR = \frac{R_E}{m_c \cdot COT} \tag{2}$$

It should be noted that a higher value of ETR provides higher performance because more mass is being collected at a lower cost of transport. Figure 8 shows a clear trend that is consistent across all configurations, angular velocities, and load times. The ETR increases in a quasi-linear fashion with load time. Interestingly, as the load time increases, the ETR appears to asymptotically approach a maximum value. A similar trend exists between ETR and angular velocity. Increasing the angular velocity from 20 to 30 RPM has a significantly larger increase in ETR than increasing it from 30 to 40 RPM in all cases. There does not appear to be a significant difference between the wide and narrow configurations C2 and C4, as both of these follow very similar trends and end up approaching the same maximum ETR values at each given ramp angle.

Note that only the 45° cases have nonzero values for C1 and C3 because they were the only ones that had nonzero excavation rates. When comparing the inward/outward churning configurations, it is obvious that the inward

churning configurations have significantly higher ETR values. This dramatic difference is illustrative of the fact that the inward churning configurations are more efficient for excavation than their outward churning counterparts while maintaining a similar cost of transport. Additionally, it is evident that increasing the ramp angle, load time, and RPM all lead to the most efficient configurations. Furthermore, for both of the outward churning configurations at the 40° and 45° ramp angles, there does not appear to be a significant difference in ETR between the four and six second load time cases at 30 and 40 RPM. These would appear to be the most efficient configuration of all settings. In a space environment, one might opt for 30 RPM to be at peak efficiency with lower total power required. The lower angular velocity would provide a lower total power requirement, which in turn would lower the mass of the spacecraft. For terrestrial applications, it would be likely to favor the faster angular velocity which would maximize the excavation rate. Ultimately it appears that there is an optimum ETR value that can be achieved with many different configurations of load time, ramp angle, and angular velocity.

In general, it was found that the inward churning configurations C2 and C4 were able to collect significantly more mass at practically the same total power while traveling at the same or greater speeds in comparison to their outward churning counterparts C1 and C3 across all load times, ramp angles, and angular velocities.

It was observed that the inward churning configurations created an elevated wake behind the front screws, directly in the path of the ramp. Conversely, the outward churning configurations diverted the sand away from the ramp, leaving a strip of undisturbed flat sand in front of the ramp. A detailed image of the wake patterns for each configuration is shown in Figure 2. It is noteworthy that the length of the depression cut by the ramp is directly proportional to the independent variable, load time. Additionally, since the outward churning configurations did not have the elevated wake, the ramp angle needed to be 45 degrees to just barely make contact with the soil. As a result, C1 and C3 were only able to collect mass at the 45 degree ramp angle. Attempts were made to collect material at 35 and 40 degrees, but were unsuccessful. This phenomenon makes it evident that having the front screws churn material inward provided a significant benefit to act as an auxiliary mechanism for excavation.

In order to compare CASPER to other ISRU excavation systems, a table of characteristic values is presented in Table 2. Note that the presented values correspond to CASPER's optimal configuration of C2, 40 RPM, 45° ramp angle, and 4 second load time. A comprehensive performance comparison between many ISRU excavators was performed by Just et al.[15] and the metrics reported in Table 2 are the same as those used in that comparison.

Table 2. CASPER Performance Metrics

Excavation rate	Depth of cut	System mass	Power requirement	Traverse speed	Simulant used
30 kg/hr	2.5 cm	3.4 kg	<30 W	10.2 m/min	Sand

CASPER yields a lower excavation rate than other discrete excavators, such as the Backhoe (100 kg/hr[35]) and Cratos (900kg/hr[36]) systems. However, CASPER delivers a serviceable excavation rate at a much lower system

mass ($\sim$ 80kg for both Backhoe[35] and Cratos[36]) and much lower power requirements ($\sim$ 200 W for Backhoe[35] and $\sim$ 100 W for Cratos[36]) while traveling at similar speeds. From these comparisons, it can be concluded that although CASPER delivers lower excavation rates than other discrete excavation systems, it does so with a much lower system mass and lower power requirements. This implies that CASPER might be better suited for extra-terrestrial applications where power and mass must be minimized. Additionally, for applications where higher excavation rates are needed, CASPER can be scaled up to accommodate those needs. However, further studies are warranted to extend current helical granular scaling laws to excavation systems.[32]

Conclusion and Future Directions

The purpose of this investigation was to characterize the excavation and mobility performance of the CASPER robot, a novel discrete scooper hybrid excavation platform. CASPER is propelled by four counter rotating Archimedes screws. These screws serve as both the mobility system, as well as augmenting the excavation system with the front screws churning up the granular media in order to be discretely scooped into the collection bin via the ramp mechanism. Four major configurations of CASPER were investigated, consisting of narrow and wide variants of inward and outward churning front screws.

The major performance parameters measured included excavation rate, power consumption, velocity, cost of transport, and a new parameter, the excavation transport rate. These dependent variables were measured over a range of the independent variables of screw angular velocity, ramp load time, ramp angle, and front screw configuration. It was found that CASPER had a peak excavation rate of around 30 kg/hr at the optimal settings of 40 RPM and 4 seconds of load time. The operational power of CASPER ranged from approximately 10-15 W for 20 RPM cases up to 20-25 W for the 40 RPM cases and exhibited very little variation with respect to load time. The velocity performance exhibited similar trends to the power consumption, with velocities ranging from 5-18 cm/s for 20-40 RPM with very little variation with load time. The cost of transport results indicated that higher angular velocities are more efficient for mobility, insofar as they move quicker for a given amount of power. The most critical parameter investigated, the excavation transport rate, aims to quantify a mixture of mobility and excavation performance that is normalized by the craft mass to enable clearer comparison between existing systems. The ETR results indicated that the optimal configuration of CASPER was a 45 degree ramp angle, 40 RPM angular velocity, with a load time of 4 seconds with the wide inward churning configuration of the front screw pontoons. This configuration had the best combination of excavation rate, power consumption, and velocity. The outward churning configurations were ineffective due to the fact that they did not create the raised section of pre-churned material in front of the ramp that the inward churning configurations did. The narrow and wide configurations were

very similar, with the wide configuration having a slight advantage in some situations.

Some promising avenues of future work have been identified during this investigation. First and foremost, increasing the scale of CASPER and operating it in a field environment would be key in determining if this architecture would be suitable for extra-terrestrial ISRU and terrestrial mining applications. One major avenue of upgrading CASPER's capability would be adding a navigation system in order to precisely control the direction of travel and correct for any deviations due to the lateral forces induced by the excavation ramp. Furthermore, adding a system to measure the excavated mass in real time would enable an investigation on how the dynamics and mobility performance of the craft is impacted as it takes on mass. Ultimately, this investigation has shown a great deal of promise for discrete scooper excavation systems, and has shown that Archimedes screw propulsion systems can substantially augment the excavation capabilities as long as the screws rotate in the proper direction to churn material towards the excavation system.

Acknowledgments

The authors would like to thank the members of the BIRTH Lab for their assistance and Arizona State University for funding.

References

[1] H. Benaroya, L. Bernold, K. M. Chua. *Journal of Aerospace Engineering* **2002**, *15*, 2 33.

[2] N. Labeaga-Martínez, M. Sanjurjo-Rivo, J. Díaz-Álvarez, J. Martínez-Frías. *Procedia Manufacturing* **2017**, *13* 794.

[3] G. Cesaretti, E. Dini, X. De Kestelier, V. Colla, L. Pambaguian. *Acta Astronautica* **2014**, *93* 430.

[4] P. Saxena, R. M. Killen, V. Airapetian, N. E. Petro, N. M. Curran, A. M. Mandell. *The Astrophysical Journal Letters* **2019**, *876*, 1 L16.

[5] S. Li, P. G. Lucey, R. E. Milliken, P. O. Hayne, E. Fisher, J.-P. Williams, D. M. Hurley, R. C. Elphic. *Proceedings of the National Academy of Sciences* **2018**, *115*, 36 8907.

[6] A. Zuppero, B. Schnitzler, T. Larson, A. Zuppero, B. Schnitzler, T. Larson. In *33rd Joint Propulsion Conference and Exhibit*. **1997** 3172.

[7] B. R. Blair, J. Diaz, M. Duke, E. Lamassoure, R. Easter, M. Oderman, M. Vaucher. *Final report to the NASA Exploration Team* **2002**.

[8] C. A. Jones, J. Klovstad, E. Judd, D. Komar. In *AIAA Scitech 2019 Forum*. **2019** 1372.

[9] I. A. Crawford. *Progress in Physical Geography* **2015**, *39*, 2 137.

[10] T. Lavoie, P. D. Spudis. In *AIAA SPACE 2016 Conference and Exposition, AIAA SPACE Forum,(AIAA 2016-5526)*. **2016** .

[11] G. Sanders. In *49th AIAA Aerospace Sciences Meeting Including the New Horizons Forum and Aerospace Exposition*. **2011** 120.

[12] G. B. Sanders, W. E. Larson. *Earth and Space 2012: Engineering, Science, Construction, and Operations in Challenging Environments* **2012**, 457–478.

[13] P. Spudis, A. Lavoie. In *AIAA Space 2011 Conference & Exposition*. **2011** 7185.

[14] R. P. Mueller, R. H. King. In *AIP conference proceedings*, volume 969. American Institute of Physics, **2008** 237–244.

[15] G. Just, K. Smith, K. Joy, M. Roy. *Planetary and Space Science* **2020**, *180* 104746.

[16] K. Skonieczny, S. J. Moreland, D. Wettergreen, W. Whittaker **2011**.

[17] D. Wettergreen, D. Jonak, D. Kohanbash, S. Moreland, S. Spiker, J. Teza, W. Whittaker. In *47th AIAA Aerospace Sciences Meeting Including The New Horizons Forum and Aerospace Exposition*. **2009** 1206.

[18] D. Wettergreen, S. Moreland, K. Skonieczny, D. Jonak, D. Kohanbash, J. Teza. *The International Journal of Robotics Research* **2010**, *29*, 12 1550.

[19] W. Reid, F. J. Pérez-Grau, A. H. Göktoğan, S. Sukkarieh. In *2016 IEEE International Conference on Robotics and Automation (ICRA)*. IEEE, **2016** 5596–5602.

[20] F. Cordes, C. Oekermann, A. Babu, D. Kuehn, T. Stark, F. Kirchner, D. Bremen. In *Proceedings of the International Symposium on Artificial Intelligence, Robotics and Automation in Space (i-SAIRAS)*. **2014** 17–19.

[21] S. Moreland, K. Skonieczny, H. Inotsume, D. Wettergreen. In *2012 IEEE Aerospace Conference*. IEEE, **2012** 1–8.

[22] X. Zeng, L. Burnoski, J. Agui, A. Wilkinson. In *45th AIAA aerospace sciences meeting and exhibit*. **2007** 1474.

[23] A. Wilkinson, A. DeGennaro. *Journal of Terramechanics* **2007**, *44*, 2 133.

[24] M. Neumeyer, B. Jones. *Journal of Terramechanics* **1965**, *2*, 4 83.

[25] K. Evans. *Journal of Sustainable Metallurgy* **2016**, *2*, 4 316.

[26] L. Ju, G. Ferri, C. Laschi, B. Mazzolai, P. Dario. In *2010 IEEE International Conference on Robotics and Automation*. IEEE, **2010** 2261–2266.

[27] A. Thoesen, S. Ramirez, H. Marvi. *AIChE Journal* **2019**, *65*, 3 894.

[28] A. Thoesen, S. Ramirez, H. Marvi. In *2018 IEEE International Conference on Robotics and Automation (ICRA)*. IEEE, **2018** 4283–4288.

[29] A. Thoesen, T. McBryan, M. Green, D. Mick, J. Martia, H. Marvi. *IEEE Robotics and Automation Letters* **2020**, *5*, 2 1319.

[30] A. Thoesen, T. McBryan, D. Mick, M. Green, J. Martia, H. Marvi. *Powder Technology* **2020**, *373* 336.

[31] A. Thoesen, T. McBryan, H. Marvi. *RSC advances* **2019**, *9*, 22 12572.

[32] A. Thoesen, T. McBryan, D. Mick, M. Green, J. Martia, H. Marvi. *Physical Review E* **2020**, *102*, 3 032902.

[33] V. Nardelli, M. Coop, J. Andrade, F. Paccagnella. *Powder Technology* **2017**, *312* 166.

[34] M. Heverly, J. Matthews, J. Lin, D. Fuller, M. Maimone, J. Biesiadecki, J. Leichty. *Journal of Field Robotics* **2013**, *30*, 6 835.

[35] P. J. van Susante, C. B. Dreyer. In *Earth and Space 2010: Engineering, Science, Construction, and Operations in Challenging Environments*, 1191–1200. **2010**.

[36] L. C. Greer, M. J. Krasowski, N. F. Prokop, D. C. Spina. Cratos: The evolution of a robotic vehicle. Technical report, NASA/TM-2013-216491, **2013**.

1 Supplementary Material

Front Power Ratio

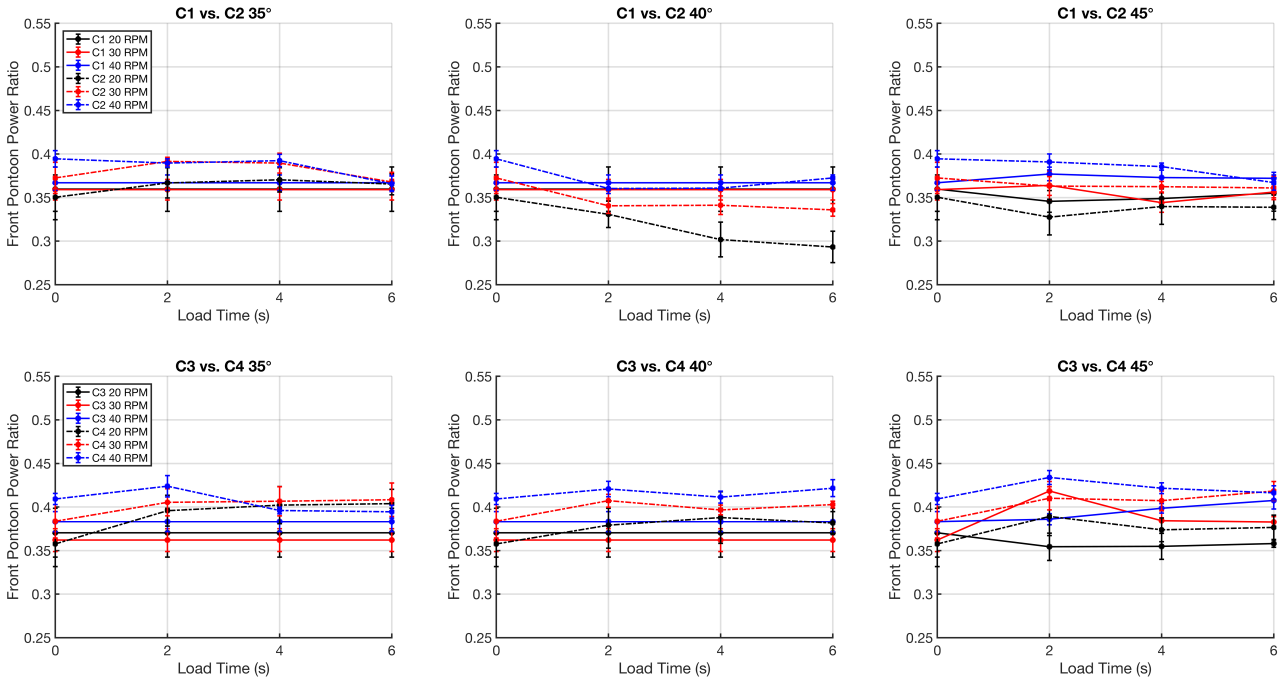

Figure 9. Comparison of the average ratio of front power vs. load time (s) between all configurations for ramp angles of 35°, 40°, and 45°, and screw rotational velocities of 20, 30, and 40 RPM.

The front power ratio is defined as the ratio between the average power consumption of the front two screws and that of all four screws, otherwise known as the mobility power. For all experimental cases, the front power ratio fluctuated very slightly between 0.35 and 0.45. Figure 9 shows that the front power ratio is essentially constant with respect to load time, and has a slight increase as RPM increases. The other variables, ramp angle, churn direction, and front pontoon width appear to have no impact upon front power ratio. One potential explanation for the fact that the front pontoons consume less power than the rear ones is that the front pontoons experienced undisturbed granular media, whereas the rear pontoons were subjected to the trailing wake of the front pontoon which was less compacted and thus, required more power to achieve the target RPM.